Research Article | Vol. 9, No. 9 | 1 Sep 2018 | BIOMEDICAL OPTICS EXPRESS 4235
Biomedical Optics EXPRESS

In vivo detection of UV-induced acute skin effects using optical coherence tomography

WEN-JU CHEN,[1,8] YAO-YU CHANG,[2,3,8] SU-CHIN SHEN,[3,4] YUA-LAN TZENG,[1] HSIANG-CHIEH LEE,[5,6] CHIH-HSUN YANG,[2,3] AND MENG-TSAN TSAI[1,2,7,*]

[1]*Department of Electrical Engineering, Chang Gung University, Taoyuan 33302, Taiwan*
[2]*Department of Dermatology, Chang Gung Memorial Hospital, Linkou and Taipei, Taiwan*
[3]*College of Medicine, Chang Gung University, Taoyuan 33302, Taiwan*
[4]*Department of Ophthalmology, Chang Gung Memorial Hospital, Taoyuan 33302, Taiwan*
[5]*Graduate Institute of Photonics and Optoelectronics, National Taiwan University, Taipei 10617, Taiwan*
[6]*Department of Electrical Engineering, National Taiwan University, Taipei 10617, Taiwan*
[7]*Medical Imaging Research Center, Institute for Radiological Research, Chang Gung University and Chang Gung Memorial Hospital at Linkou, Taoyuan 33302, Taiwan*
[8]*These authors equally contributed to this work.*
**mttsai@mail.cgu.edu.tw*

Abstract: Ultraviolet (UV) rays have been identified as a carcinogen with long-term irradiation and are an important risk factor for skin cancer. Here, we report the use of optical coherence tomography/optical coherence tomography angiography (OCT/OCTA) to study acute UV-induced effects on skin *in vivo*. To understand the relationship between the acute effects and irradiated UV power density, three groups were irradiated with different power densities in our experiments. Furthermore, the same skin area was repeatedly scanned with OCT during UV irradiation to investigate the progress of the induced acute effects and after irradiation for observation of skin recovery. Subsequently, the OCT/OCTA results were quantitatively analyzed to acquire skin thickness and blood-vessel density for comparison. UV-induced acute effects on morphology and microcirculation can be identified from OCT/OCTA results, which showed the increases in the skin thickness and blood-vessel density and even severe damage types such as blisters. The results of quantitative analyses also illustrated that the severity of damage induced by UV irradiation can be distinguished and the skin recovery can be monitored with OCT. Our results indicate that OCT can be a promising tool for early detection of UV-induced acute skin damage.

OCIS codes: (170.4500) Optical coherence tomography; (170.2655) Functional monitoring and imaging; (170.3880) Medical and biological imaging.

References and links

1. Y. Tong, M. A. Smith, and S. B. Tucker, "Chronic ultraviolet exposure-induced p53 gene alterations in Sencar mouse skin carcinogenesis model," J. Toxicol. Environ. Health **51**(3), 219–234 (1997).
2. T. Schwarz, "25 years of UV-induced immunosuppression mediated by T cells-from disregarded T suppressor cells to highly respected regulatory T cells," Photochem. Photobiol. **84**(1), 10–18 (2008).
3. F. S. Weill, E. M. Cela, A. Ferrari, M. L. Paz, J. Leoni, and D. H. González Maglio, "Skin exposure to chronic but not acute UV radiation affects peripheral T-cell function," J. Toxicol. Environ. Health A **74**(13), 838–847 (2011).
4. R. P. Sinha and D. P. Häder, "UV-induced DNA damage and repair: a review," Photochem. Photobiol. Sci. **1**(4), 225–236 (2002).
5. R. P. Rastogi, A. Richa, M. B. Kumar, Tyagi, and R. P. Sinha, "Molecular mechanisms of ultraviolet radiation-induced DNA damage and repair," J. Nucleic Acids **2010**, 1 (2010).
6. J. D'Orazio, S. Jarrett, A. Amaro-Ortiz, and T. Scott, "UV radiation and the skin," Int. J. Mol. Sci. **14**(6), 12222–12248 (2013).
7. D. Huang, E. A. Swanson, C. P. Lin, J. S. Schuman, W. G. Stinson, W. Chang, M. R. Hee, T. Flotte, K. Gregory, C. A. Puliafito, and J. G. Fujimoto, "Optical coherence tomography," Science **254**(5035), 1178–1181 (1991).
8. A. G. Podoleanu, "Optical coherence tomography," J. Microsc. **247**(3), 209–219 (2012).

#332680 https://doi.org/10.1364/BOE.9.004235
Journal © 2018 Received 29 May 2018; revised 13 Jul 2018; accepted 2 Aug 2018; published 14 Aug 2018

Biomedical Optics EXPRESS

9. G. Liu, A. J. Lin, B. J. Tromberg, and Z. Chen, "A comparison of Doppler optical coherence tomography methods," Biomed. Opt. Express **3**(10), 2669–2680 (2012).
10. R. A. Leitgeb, R. M. Werkmeister, C. Blatter, and L. Schmetterer, "Doppler optical coherence tomography," Prog. Retin. Eye Res. **41**, 26–43 (2014).
11. S. Makita, Y. Hong, M. Yamanari, T. Yatagai, and Y. Yasuno, "Optical coherence angiography," Opt. Express **14**(17), 7821–7840 (2006).
12. C. L. Chen and R. K. Wang, "Optical coherence tomography based angiography [Invited]," Biomed. Opt. Express **8**(2), 1056–1082 (2017).
13. M. Yamanari, S. Makita, Y. Lim, and Y. Yasuno, "Full-range polarization-sensitive swept-source optical coherence tomography by simultaneous transversal and spectral modulation," Opt. Express **18**(13), 13964–13980 (2010).
14. M. Pircher, C. K. Hitzenberger, and U. Schmidt-Erfurth, "Polarization sensitive optical coherence tomography in the human eye," Prog. Retin. Eye Res. **30**(6), 431–451 (2011).
15. A. Curatolo, M. Villiger, D. Lorenser, P. Wijesinghe, A. Fritz, B. F. Kennedy, and D. D. Sampson, "Ultrahigh-resolution optical coherence elastography," Opt. Lett. **41**(1), 21–24 (2016).
16. P. Meemon, J. Yao, Y. J. Chu, F. Zvietcovich, K. J. Parker, and J. P. Rolland, "Crawling wave optical coherence elastography," Opt. Lett. **41**(5), 847–850 (2016).
17. M. Mogensen, L. Thrane, T. M. Jørgensen, P. E. Andersen, and G. B. Jemec, "OCT imaging of skin cancer and other dermatological diseases," J. Biophotonics **2**(6-7), 442–451 (2009).
18. C. A. Banzhaf, L. Themstrup, H. C. Ring, M. Mogensen, and G. B. Jemec, "Optical coherence tomography imaging of non-melanoma skin cancer undergoing imiquimod therapy," Skin Res. Technol. **20**(2), 170–176 (2014).
19. M. T. Tsai, C. H. Yang, S. C. Shen, Y. J. Lee, F. Y. Chang, and C. S. Feng, "Monitoring of wound healing process of human skin after fractional laser treatments with optical coherence tomography," Biomed. Opt. Express **4**(11), 2362–2375 (2013).
20. M. T. Tsai, D. R. Li, and M. C. Chan, "Non-invasive image-guided laser microsurgery by a dual-wavelength fiber laser and an integrated fiber-optic multi-modal system," Opt. Lett. **41**(20), 4847–4850 (2016).
21. L. M. Vasquez-Pinto, E. P. Maldonado, M. P. Raele, M. M. Amaral, and A. Z. de Freitas, "Optical coherence tomography applied to tests of skin care products in humans--a case study," Skin Res. Technol. **21**(1), 90–93 (2015).
22. H. Morsy, S. Kamp, L. Thrane, N. Behrendt, B. Saunder, H. Zayan, E. A. Elmagid, and G. B. E. Jemec, "Optical coherence tomography imaging of psoriasis vulgaris: correlation with histology and disease severity," Arch. Dermatol. Res. **302**(2), 105–111 (2010).
23. M. Mogensen, H. A. Morsy, B. M. Nurnberg, and G. B. E. Jemec, "Optical coherence tomography imaging of bullous diseases," J. Eur. Acad. Dermatol. Venereol. **22**(12), 1458–1464 (2008).
24. J. K. Barton, K. W. Gossage, W. Xu, J. R. Ranger-Moore, K. Saboda, C. A. Brooks, L. D. Duckett, S. J. Salasche, J. A. Warneke, and D. S. Alberts, "Investigating sun-damaged skin and actinic keratosis with optical coherence tomography: a pilot study," Technol. Cancer Res. Treat. **2**(6), 525–535 (2003).
25. V. R. Korde, G. T. Bonnema, W. Xu, C. Krishnamurthy, J. Ranger-Moore, K. Saboda, L. D. Slayton, S. J. Salasche, J. A. Warneke, D. S. Alberts, and J. K. Barton, "Using optical coherence tomography to evaluate skin sun damage and precancer," Lasers Surg. Med. **39**(9), 687–695 (2007).
26. T. Gambichler, B. Künzlberger, V. Paech, A. Kreuter, S. Boms, A. Bader, G. Moussa, M. Sand, P. Altmeyer, and K. Hoffmann, "UVA1 and UVB irradiated skin investigated by optical coherence tomography in vivo: a preliminary study," Clin. Exp. Dermatol. **30**(1), 79–82 (2005).
27. M. T. Tsai, J. W. Zhang, K. C. Wei, C. K. Yeh, and H. L. Liu, "Assessment of temporary cerebral effects induced by focused ultrasound with optical coherence tomography angiography," Biomed. Opt. Express **9**(2), 507–517 (2018).
28. A. Mariampillai, B. A. Standish, E. H. Moriyama, M. Khurana, N. R. Munce, M. K. Leung, J. Jiang, A. Cable, B. C. Wilson, I. A. Vitkin, and V. X. Yang, "Speckle variance detection of microvasculature using swept-source optical coherence tomography," Opt. Lett. **33**(13), 1530–1532 (2008).

1. Introduction

Previous reports have indicated that exposure to solar radiation has a high risk of deleterious effects on skin, which may further result in skin cancers such as basal/squamous-cell carcinoma (BCC/SCC) and cutaneous malignant melanoma [1–3]. Moreover, excessive UV exposure induces genetic mutants as a result of damage to the cellular DNA of skin, and it is a key factor in nonmelanoma skin cancers and BCC/SCC [4]. The UV spectrum ranges from 10 to 400 nm and can be roughly divided into three sub-bands: UVA, UVB, and UVC. The long-term effects of UV radiation have been intensively studied in past reports [5]. For example, long-term exposure to UVA rays makes skin cells age faster and causes damages to DNA. UVB rays also cause DNA damage and may further result in skin cancer with long-term irradiation. In contrast, the UVC component in solar light is blocked by the atmosphere.

Biomedical Optics EXPRESS

Therefore, UVA and UVB are the main causes of skin damage and cancer with long-term irradiation, and they cover a spectral range of 280–400 nm [6].

Optical coherence tomography (OCT), consisting of an optical interferometer, receives backscattered or reflected signals from biological tissue to image its two/three-dimensional microstructure [7,8]. Since OCT is based on the scattering properties of biological tissue, no extra fluorescence dye or contrast agent is required. In addition to obtaining tissue structure, functional imaging abilities were also intensively developed, including the abilities to determine blood-flow velocity [9,10], angiography [11,12], birefringence [13,14], and elasticity [15,16]. In previous studies, OCT has been widely applied for dermatologic applications such as skin cancer [17,18], laser treatment [19,20], cosmetics [21], and skin disorders [22,23]. Barton *et al.* investigated skin damage induced by the sun and actinic keratosis in 20 human subjects with OCT. It was noted that the thickness of the epidermis layer of sun-damaged skin increased, resulting in stronger attenuation along the tissue depth. Additionally, the thicknesses of normal, sun-damaged, and actinic-keratosis skin were statistically compared, indicating that the thickness could be a promising indicator for evaluating skin condition [24,25]. Gambichler *et al.* used OCT and histology to study UVA1/UVB-induced acute skin effects. In their study, the epidermis thickness and the scattering coefficients of epidermis and dermis layers were evaluated for UVA-exposed, UVB-exposed, and unexposed skin sites. The results indicated that both UVA and UVB irradiation have an impact on the epidermis thickness [26].

Although the abovementioned studies used OCT for investigating UV-induced skin damage and sunburns, the dependence of irradiated power on the damage, the acute effects of UV irradiation, and skin recovery after UV irradiation are not well investigated. In this study, we report the use of OCT and OCT angiography (OCTA) to investigate the acute effects of UV irradiation with different power densities on the skin. To understand changes in the microstructure and microcirculation induced by UV irradiation, we compare OCT and OCTA results obtained at different time points including time points during and after UV irradiation. Finally, we demonstrate quantitative analyses of the skin thickness and blood-vessel density after UV irradiation with different power densities.

2. Experimental setup and method

2.1 OCT system

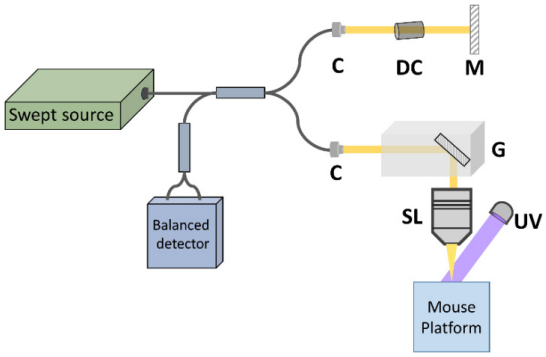

Fig. 1. Schematic diagram of the OCT setup combined with UV irradiation equipment. C: collimator; DC: dispersion compensator; M: mirror; G: two-axis galvanometer; SL: scanning lens.

In this study, a swept-source OCT (SS-OCT) system was developed for investigating the UV-induced acute effects on skin, and the SS-OCT system setup is similar to that in our previous study, as shown in Fig. 1 [27]. A 1060-nm swept source (SSOCT-1060, AXSUN Technologies Inc., MA, USA) with a scanning bandwidth of 100 nm was utilized,

Biomedical Optics EXPRESS

corresponding to a longitudinal resolution of 5 μm in air. The OCT system is based on a Michelson interferometer with an extra fiber coupler having a coupling ratio of 50/50 to achieve balanced detection. The analog signal from the balanced detector (PDB460C, Thorlabs Inc., NJ, USA) was converted by a digitizer (ATS-9350, Alazar Technologies Inc., QC, Canada) with a sampling rate of 500 MHz. Additionally, the analog interference spectrum was resampled through an external k-clock signal from the light source for wavelength calibration. For scanning mouse skin, a scanning lens (LSM02-BB, Thorlabs Inc., NJ, USA) was inserted in the sample arm of the interferometer, providing a transverse resolution of ~6 μm. The scan rate of the swept source is 100 kHz, which provided a frame rate of 100 Hz.

2.2 Experimental animal and method

To study UV-induced skin effects, mice (C57 wild-type) with the age of 7–8 weeks were used as the experimental animals. The experimental procedure was approved by the Institutional Animal Care and Use Committee (IACUC) of Chang Gung University. The mice were anesthetized on a special mount with isoflurane, and the ear was unfolded and fixed on a glass plate. The UV light source covers a spectral range of 280–400 nm with a maximum output power of 50 W. To investigate the acute effects with different power densities, three groups (n = 5 for each group) were used in our experiment: Group 1 was exposed to a power density of 0.14 W/cm^2, Group 2 to a power density of 0.61 W/cm^2, and Group 3 to a power density of 2.18 W/cm^2. The irradiation period for each group was 9 minutes and the corresponding energy densities are 75.6, 329.4, and 1177.2 J/cm^2, respectively. In our experiments, an accelerated study design was implemented since the power density of the UV irradiation during routine sun light exposure is low. UV irradiation with a low power density requires much longer study time in order to investigating the consequence of UV irradiation on skin. Thus, the higher power densities were performed in the study. For UV irradiation, the entire mouse-ear area was illuminated, and the same ear skin area was repeatedly scanned with OCT to acquire 3D microstructural and micro-angiographic images for comparison during and after UV irradiation. To repeatedly scan the same skin area, the OCT scanning range was carefully aligned to a specific location of mouse ear (for example, the bifurcation of vessels) before each measurement and the same voltages for the two-axis galvanometer were applied to scan the same area. To acquire OCTA images, speckle variance among sequential B-scans obtained at the same location was estimated [28]. In our system, two sequential B-scans at the same location were performed for OCTA imaging, and the larger speckle variation corresponded to the blood flow. Therefore, 3D OCT and OCTA images can be simultaneously obtained for each scan. Each 3D OCT imaging data set exhibits a pixel density of 1000 × 500 × 1024 pixels (X × Y × Z) covering a physical range of 3 × 3 × 2 mm^3, respectively.

3. Experimental results

Since UV irradiation with different power densities may cause different acute effects on skin, each mouse skin was exposed to a specific power-density level for 9 minutes. Firstly, UV irradiation with a power density of 0.14 W/cm^2 was performed. To observe the progress of skin effects due to UV irradiation, the same skin area was repeatedly scanned with OCT at various time points. Figures 2(a)–(g) show representative 2D-OCT images of the same skin area obtained before UV irradiation and after UV irradiation with a power density of 0.14 W/cm^2 for 1.5, 3.0, 4.5, 6.0, 7.5, and 9.0 min. In Fig. 2(a), different skin layers can be identified including the epidermis, dermis, and auricular cartilage. No significant change in skin structure could be identified with the increase in irradiation period. In addition to the investigation of acute response during UV irradiation, the same skin area was continuously scanned to observe the recovery progress, as shown in Figs. 2(h)–(k). Similarly, no obvious

Biomedical Optics EXPRESS

acute effect on the skin microstructure could be identified after low-power-density UV irradiation.

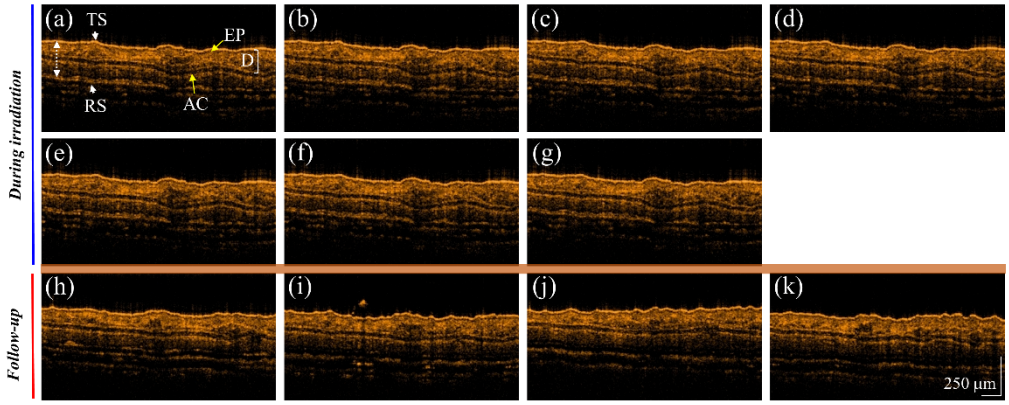

Fig. 2. *In vivo* OCT images of mouse-ear skin obtained (a) before UV irradiation, and after UV irradiation with a power density of 0.14 W/cm^2 for (b) 1.5 min, (c) 3 min, (d) 4.5 min, (e) 6 min, (f) 7.5 min, and (g) 9 min. After UV irradiation, the same skin area was repeatedly scanned at different time points of (h) 1 day, (i) 2 days, (j) 3 days, and (k) 4 days from irradiation for follow-up observation. The yellow arrows indicate the different layer structures including the epidermis (EP), dermis (D), and auricular cartilage (AC). TS: top surface and RS: rear surface.

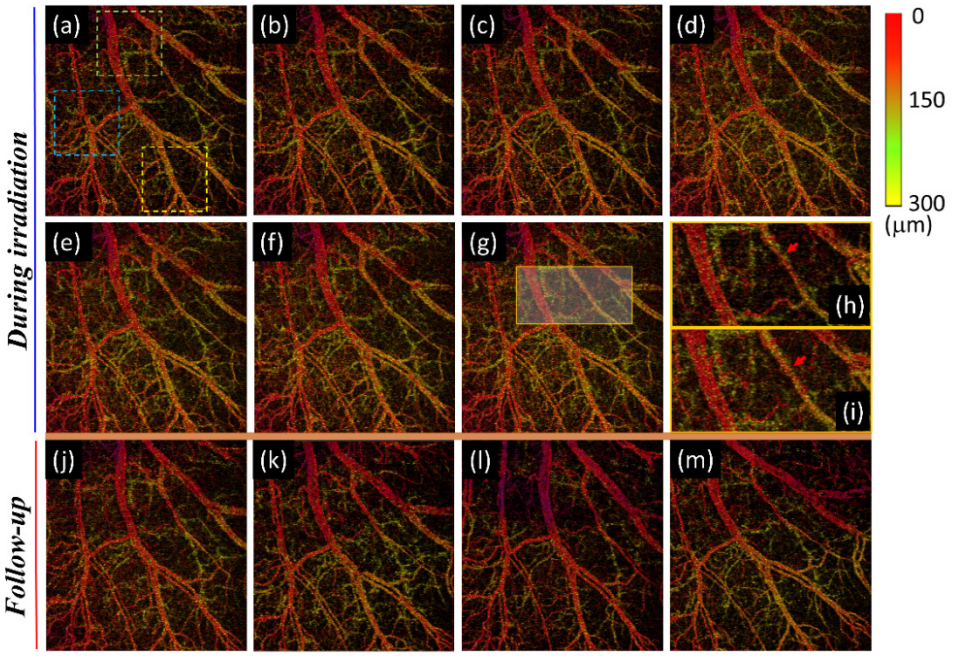

Fig. 3. Corresponding color-coded, projection-view OCTA results of Fig. 2. Images were obtained (a) before UV irradiation, and after UV irradiation with a power density of 0.14 W/cm^2 for (b) 1.5 min, (c) 3 min, (d) 4.5 min, (e) 6 min, (f) 7.5 min, and (g) 9 min. (h) and (i) show enlarged views of (a) and (g) in the area indicated by the golden square in (g). After UV irradiation, the same skin area was continuously scanned at different time points of (j) 1 day, (k) 2 days, (l) 3 days, and (l) 4 days from irradiation for follow-up observation. The vessel size and density increased after UV irradiation and recovered in one day after irradiation. Each angiographic image covers a physical range of 3 × 3 mm^2.

Biomedical Optics EXPRESS

The corresponding projection-view OCTA results of Fig. 2 are shown in Fig. 3 which is color-coded by depth. Each angiographic image covers a physical range of 3 × 3 mm^2. Figure 3(a) was obtained before UV irradiation, and Figs. 3(b)–(g) show projection-view OCTA results obtained after UV irradiation for 1.5, 3, 4.5, 6, 7.5, and 9 min, respectively. Figures 3(h) and (i) show enlarged views of the OCTA images in Figs. 3(a) and (g) in the area indicated by the golden square in Fig. 3(g). Compared to the result of Fig. 3(a), it is noted that the vessel size and density increased after UV irradiation, as can be confirmed from Figs. 3(h) and (i). The red arrows indicate the same blood vessel with different diameters. The increase in vessel diameter is due to skin inflammation induced by UV irradiation. Inflammation causes the increased blood flow and further leads to the vessel expansion, presenting a symptom of redness. As increasing the irradiation period, the vessels in the deeper depth range, representing in the yellow-green color, became visualized. That was also due to the increased blood flow induced by UV irradiation, leading to vessel expansion. However, such vessel expansion gradually reversed after UV irradiation. Figures 3(j)–(m) show the corresponding OCTA results of Figs. 2(h)–2(k). The images show that the acute effects on microcirculation induced by UV irradiation disappeared after 24 h, illustrating that such low-power-density irradiation only causes temporal effects on vessels, which can be reversed in one day.

Subsequently, the power density of UV irradiation was increased to 0.61 W/cm^2, and the same experimental procedure was repeated. Figures 4(a)–(g) show the OCT images of another mouse-ear skin obtained before irradiation and after UV irradiation for 1.5, 3.0, 4.5, 6.0, 7.5, and 9.0 min, respectively. The OCT images in Fig. 4 show similar results as those in Fig. 2. It is difficult to identify the difference in the results obtained before and after irradiation with the naked eye. Furthermore, the recovery process after UV irradiation was monitored with OCT, and the results show no significant change in skin microstructure when the irradiated power density was increased to 0.61 W/cm^2.

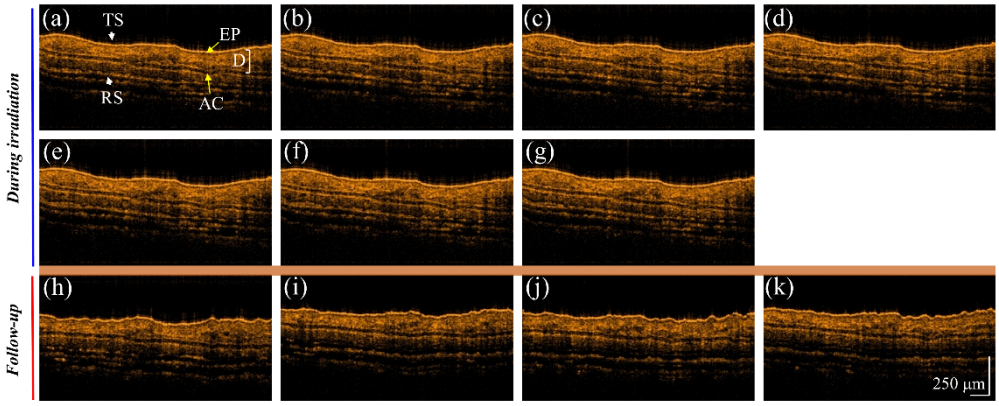

Fig. 4. *In vivo* OCT images of mouse-ear skin obtained (a) before UV irradiation, and after UV irradiation with a power density of 0.61 W/cm^2 for (b) 1.5 min, (c) 3 min, (d) 4.5 min, (e) 6 min, (f) 7.5 min, and (g) 9 min. After UV irradiation, the same skin area was scanned at different time points of (h) 1 day, (i) 2 days, (j) 3 days, and (k) 4 days from irradiation for follow-up observation. The yellow arrows indicate the different layer structures including the epidermis (EP), dermis (D), and auricular cartilage (AC). TS: top surface and RS: rear surface.

Additionally, the corresponding OCTA results are shown in Fig. 5 which is color-coded by depth. Figures 5(a)–(g) and 5(j)–(m) represent the corresponding projection-view OCTA images of Figs. 4(a)–(g) and 4(h)–(k), respectively. The blood vessels in the area indicated by the golden square in Fig. 5(g) were enlarged in comparison to those in the same area in Figs. 5(a), as shown in Figs. 5(i) and (h), respectively. Similar to the results in Fig. 3, the vessels in the deeper depth range, shown in the yellow-green color, emerged after irradiation and

Biomedical Optics EXPRESS

gradually disappeared with time. The results illustrate that some vessels became visible after UV irradiation because of skin inflammation, implying that UV irradiation with a higher power density caused skin inflammation, increasing the vessel size and density. Moreover, the same skin area was repeatedly imaged with OCT to investigate the skin recovery. In Fig. 5(j), the vessel density reduced, and Fig. 5(m) shows a similar microvascular pattern to Fig. 5(a), illustrating that the acute effect can be greatly reduced 4 days after UV irradiation.

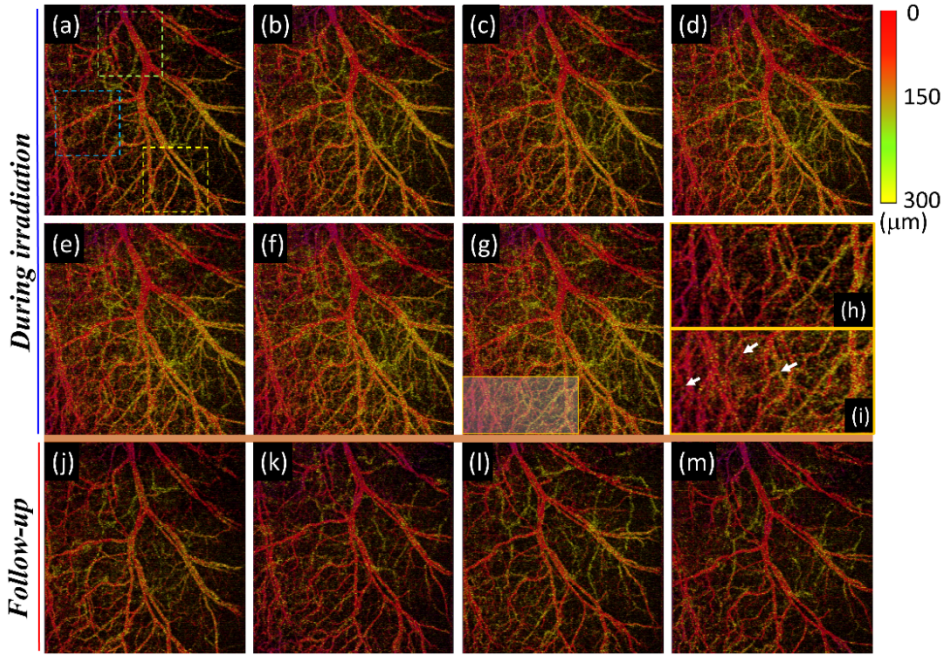

Fig. 5. Corresponding color-coded, projection-view OCTA results of Fig. 4. Images were obtained (a) before UV irradiation, and after UV irradiation with a power density of 0.61 W/cm^2 for (b) 1.5 min, (c) 3 min, (d) 4.5 min, (e) 6 min, (f) 7.5 min, and (g) 9 min. (h) and (i) show enlarged views of (a) and (g) in the area indicated by the golden square in (g). After UV irradiation, the same skin area was continuously scanned at different time points of (j) 1 day, (k) 2 days, (l) 3 days, and (l) 4 days from irradiation for follow-up observation. The results illustrate that UV irradiation with a higher power density caused skin inflammation, increasing the vessel size and density. Each angiographic image covers a physical range of 3 × 3 mm^2.

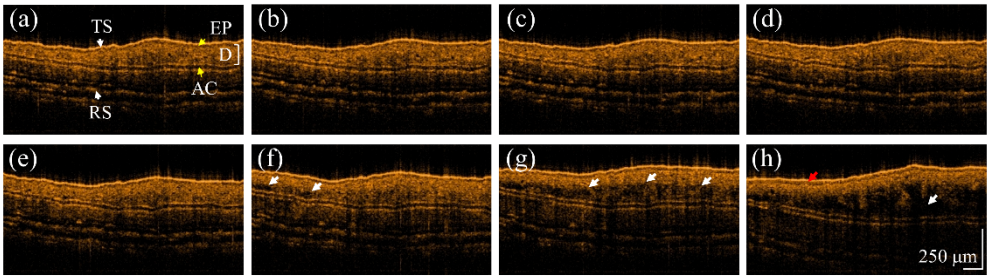

Fig. 6. *In vivo* OCT images of mouse-ear skin obtained (a) before UV irradiation, and after UV irradiation with a power density of 2.18 W/cm^2 for (b) 1.5 min, (c) 3 min, (d) 4.5 min, (e) 6 min, (f) 7.5 min, and (g) 9 min. (h) The same skin area scanned 1 h after UV irradiation. The yellow arrows indicate the different layer structures including the epidermis (EP), dermis(D), and auricular cartilage (AC). The white arrows in (f)–(h) indicate the blisters induced by the strong UV irradiation.

For Group 3, the power density of UV irradiation was increased to 2.18 W/cm^2. Figures 6(a)–(g) show 2D OCT images of mouse-ear skin obtained before irradiation and after UV

Biomedical Optics EXPRESS

irradiation for 1.5, 3.0, 4.5, 6.0, 7.5, and 9.0 min, respectively. The backscattered intensity of the mouse-ear skin started to become weaker after irradiation for 6 min, as indicated by the white arrows in Figs. 6(f) and 6(g). The same skin area was scanned with OCT after 1 h, as shown in Fig. 6(h). Compared with Fig. 6(a), the thicknesses of the epidermis and dermis significantly increased. Moreover, the weaker backscattered area, as indicated by the white arrow in Fig. 6(h), also increased because of the occurrence of blisters, which resulted in stronger attenuation. The results show that UV irradiation with a higher power density causes severer damage types such as blisters and inflammation. The corresponding OCTA results of Fig. 6 are shown in Fig. 7. Similarly, the vessel distribution became denser after 1.5-min irradiation but decreased after 7.5-min irradiation. As shown in Fig. 6, the blisters also blurred the OCTA results because they increased the optical absorption and limited the optical penetration. Since the speckle variance between sequential B-scans obtained in the same area was estimated to acquire an OCTA image, the weaker OCT intensity due to the attenuation resulting from blisters made angiography difficult. Therefore, the vessel density reduced after 7.5-min irradiation, as shown in Fig. 7(g). However, the appearance of blisters can be detected with OCT/OCTA. Here, the follow-up results are not shown because the blisters became bigger with time, making angiography difficult.

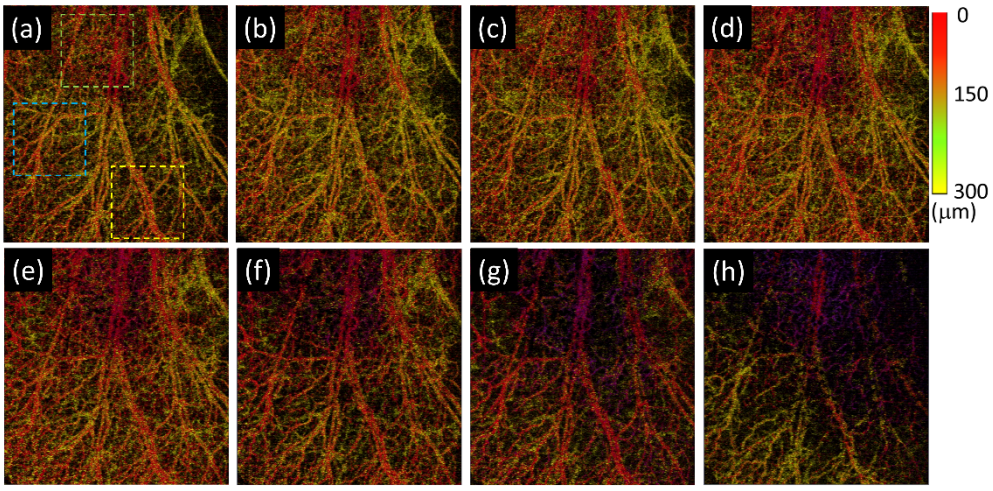

Fig. 7. Corresponding color-coded, projection-view OCTA results of Fig. 6. Images were obtained (a) before UV irradiation, and after UV irradiation with a power density of 2.18 W/cm^2 for (b) 1.5 min, (c) 3 min, (d) 4.5 min, (e) 6 min, (f) 7.5 min, and (g) 9 min. (h) The same skin area scanned 1 h after UV irradiation. Each angiographic image covers a physical range of 3 × 3 mm^2.

Figure 8 shows the corresponding photographs of Figs. 3, 5 and 7 taken (a)-(c) before and (d)-(f) at the time point of 1 h after UV irradiation stopped, respectively. For the cases of the lower power densities of 0.14 and 0.61 W/cm^2, the acute effects are not obvious with the naked eye. However, when a high power energy of 2.18 W/cm^2 was applied, an erythema can be found in Fig. 8(f). In comparison to the corresponding photographs, the OCT results (as shown in Figs. 3, 5, and 7) can visualize the details of microcirculation and erythema which are difficult to be identified with the naked eye for the lower power-density cases. The OCT/OCTA results illustrate that OCT can be used for early detection of UV-induced acute skin effects.

Biomedical Optics EXPRESS

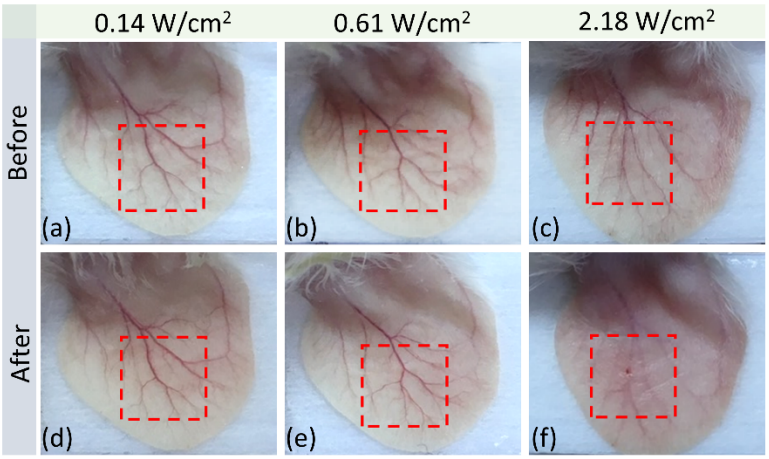

Fig. 8. Corresponding photographs of Figs. 3, 5, and 7 taken (a)-(c) before and (d)-(f) at the time point of 1 h after UV irradiation stopped. The red squares indicate the OCT scanning area.

4. Discussion and conclusion

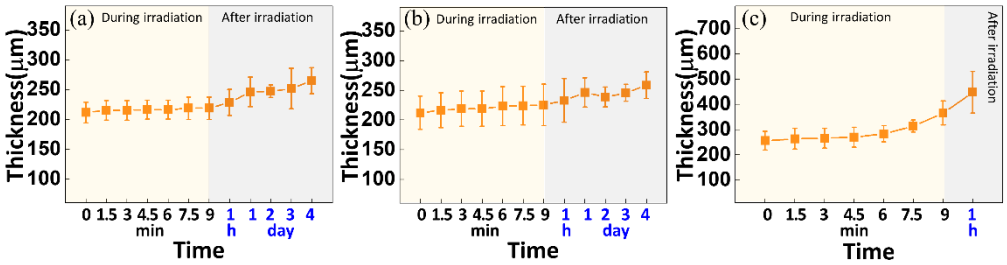

Fig. 9. Estimation results of skin thickness from Figs. 2, 4, and 6. The power densities of UV irradiation are (a) 0.14 W/cm^2, (b) 0.61 W/cm^2, and (c) 2.18 W/cm^2.

To further investigate the acute effects induced by UV irradiation quantitatively, the skin thickness and vessel density were evaluated. To determine the skin thickness, we estimated the total thickness of mouse-ear skin from OCT images, as indicated by the vertical arrow in Fig. 2(a). To estimate the thickness of mouse skin, twenty-one A-scans at different locations were manually selected from every 2D cross-sectional OCT image, and the thicknesses between the top and bottom surfaces of the mouse skin at individual A-scan locations can be determined afterward. Then, the measured mouse skin thicknesses at these twenty-one transverse locations in each 2D OCT image were averaged to obtain a mean value of skin thickness. Additionally, the method for estimating the vessel density is similar to that in the previous report [27]. Three subareas in each OCTA image for each group (as marked by colored squares in Figs. 3, 5, and 7) were chosen to estimate an average vessel density. Each square area approximately equals 1 mm^2. Figures 9 and 10 show the estimation results of skin thickness and vessel density, respectively. In Fig. 9(a), there was no significant change in skin thickness during UV irradiation, but the average skin thickness increased after irradiation. In contrast, when the power density was increased to 0.61 W/cm^2, as shown in Fig. 9(b), the skin thickness gradually increased during UV irradiation as well as after irradiation. Compared to the previous two cases, Fig. 9(c) illustrates that the skin thickness slightly increased after 6-min irradiation and significantly increased after 7.5-min irradiation. Even after irradiation, the thickness continued to increase. The acute skin effect induced by UV irradiation caused edema, resulting in the increase in skin thickness. Additionally, the skin thickness significantly becomes much thicker due to the occurrence of blisters after UV irradiation with

Biomedical Optics EXPRESS

a high power density, as shown in Fig. 9(c). The results illustrate that UV irradiation caused skin thickening, and such an acute effect cannot be reduced in days. Moreover, irradiation with a high power density resulted in severer damage types such as blisters, making the skin swollen and inflamed.

The average vessel densities for the three power densities are shown in Fig. 10. From Fig. 10(a), it can be found that the vessel density gradually increased (from 27.2% to 32.2% in 9 minutes) during UV irradiation but started to decrease after irradiation. The vessel density can be recovered as that before UV irradiation after 4 days. Compared to the results of Fig. 10(a), Fig. 10(b) presents a significant increase in the vessel density (from 26.3% to 38.1% in 9 minutes) during irradiation, implying that irradiation with a higher power density causes a more severe skin reaction. However, the results also show that such an acute effect can disappear in 4 days. For the highest power density, the vessel density also increased for 1.5-min irradiation (from 38.2% to 46.1%) but started to decrease at 6-min irradiation, which is in agreement with the results of Fig. 9(c). As mentioned previously, the decrease in the vessel density was due to the appearance of blisters, causing stronger attenuation and blurring OCTA results. Even after 1 h, the blister size continuously increased, making the attenuation of the OCT signal stronger. However, it is noted that OCT and OCTA are able to evaluate the UV-induced effects on microstructure and microcirculation, and the induced severer damage types such as blisters can also be detected.

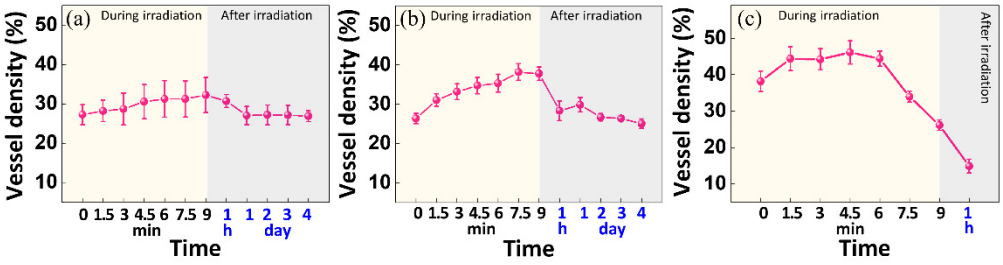

Fig. 10. Estimation results of vessel density from Figs. 3, 5, and 7. The power densities of UV irradiation are (a) 0.14 W/cm^2, (b) 0.61 W/cm^2, and (c) 2.18 W/cm^2.

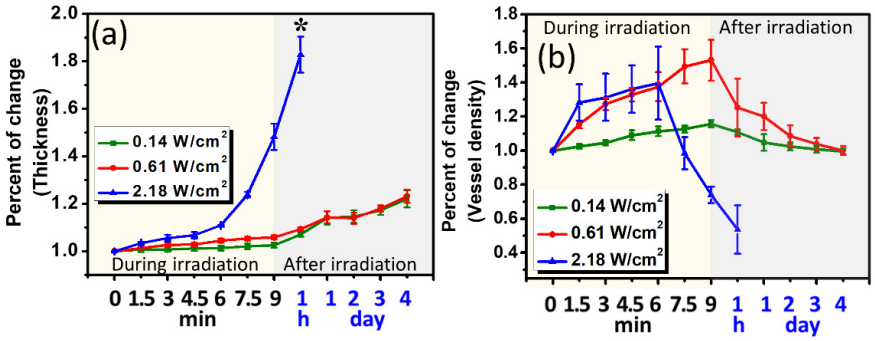

Fig. 11. The estimated PC values of (a) skin thickness and (b) vessel density for different power densities including 0.14, 0.61, and 2.18 W/cm^2. The asterisk indicates $p<0.05$.

To further investigate the changes in skin thickness and microcirculation, the experimental results from animals (n = 5 for each group) were analyzed. Since the skin thicknesses and vessel densities varied between different mice, the percent of change (PC) of skin thickness/vessel density other than the absolute values of these two parameters was estimated for comparison. Here, PC is defined as the change as a percent of the original value. Figures 11(a) and 11(b) show the mean PC values of the thickness and the vessel density for three power-density groups. In Fig. 11(a), the PC value slightly increased during irradiation with

Biomedical Optics EXPRESS

the low power densities, such as 0.14 or 0.61 W/cm^2 and kept increasing after the irradiation was stopped. In contrast, the PC value rapidly increased after irradiation with the power-density level of 2.18 W/cm^2 for 6 min because of the occurrence of blisters. Moreover, the standard deviation of PC became larger after irradiation for 9 min and at the time point of 1 h after irradiation, resulting from the difference in the sizes of the induced blisters. Moreover, one-way analysis of variance (ANOVA) was performed to evaluate the statistical significance of differences in the PC values of thickness at the time point of 1 hour after UV irradiation with three power-density levels. The estimated possibility value (p) is less than 0.05 as marked by the asterisk in Fig. 11(a), representing the difference is statically significant. In Fig. 11(b), the PC value of the vessel density gradually decreased after the UV irradiation stopped (i.e. at the time point of 9 min) for the 0.14 W/cm^2 and 0.61 W/cm^2 cases. Additionally, the standard deviation in the vessel density results significantly became larger that was probably due to the severity of induced erythema varied among individuals. For the curve of 2.18 W/cm^2 in Fig. 11(b), the PC value started to decrease after irradiation for 6 min, resulting from the occurrence of blisters limited optical penetration and blurred OCTA results.

In conclusion, we demonstrated the use of OCT/OCTA to study acute skin effects due to UV irradiation. Irradiation was performed with different power densities, and the induced acute effects were investigated. Furthermore, the progress of UV-induced effects during UV irradiation was studied as well as the progress of skin recovery after irradiation. It is noted that UV irradiation with a low power density may cause the increase of skin thickness and skin inflammation, resulting in the increase of blood-vessel density. The results also show that the acute effect on microcirculation induced by a low power density can be recovered in days, but a longer time is required for the recovery of skin thickness. In contrast, a high power density may cause severer damage types such as blisters and skin swelling. Such a blister structure also results in the increase of thickness and attenuation of the OCT signal, blurring OCTA images. However, the blisters can be detected from OCT and OCTA. Our experimental results demonstrate that OCT/OCTA can be a promising tool for early detection of UV-induced acute effects and monitoring skin recovery from UV-induced damage.

Funding

Chang Gung Memorial Hospital, Taiwan (CMRPD 2F0132 and CMRPD 2F0131); Ministry of Science and Technology of the Republic of China (ROC), Taiwan (MOST 106-2221-E-182A-001, 105-2221-E182-016-MY3, 107-2636-E-002-003, and 105-2627-M-007-007).

Disclosures

The authors declare that there are no conflicts of interest related to this article.